J|A|C|S ARTICLES

Published on Web 06/24/2010

Molecular Mechanisms in Morpholino−DNA Surface Hybridization

Ping Gong,[†] Kang Wang,[‡] Yatao Liu,[‡] Kenneth Shepard,[§] and Rastislav Levicky*[,‡]

Seventh Sense Biosystems Inc., 101 Binney Street, Cambridge, Massachusetts 02142, Chemical and Biological Engineering, Polytechnic Institute of New York University, 6 MetroTech Center, Brooklyn, New York 11201, and Electrical Engineering, Columbia University, 500 West 120th Street, New York, New York 10027

Received February 1, 2010; E-mail: rlevicky@poly.edu

Abstract: Synthetic nucleic acid mimics provide opportunity for redesigning the specificity and affinity of hybridization with natural DNA or RNA. Such redesign is of great interest for diagnostic applications where it can enhance the desired signal against a background of competing interactions. This report compares hybridization of DNA analyte strands with morpholinos (MOs), which are uncharged nucleic acid mimics, to the corresponding DNA−DNA case in solution and on surfaces. In solution, MO−DNA hybridization is found to be independent of counterion concentration, in contrast to DNA−DNA hybridization. On surfaces, when immobilized MO or DNA "probe" strands hybridize with complementary DNA "targets" from solution, both the MO−DNA and DNA−DNA processes depend on ionic strength but exhibit qualitatively different behaviors. At lower ionic strengths, MO−DNA surface hybridization exhibits hallmarks of kinetic limitations when separation between hybridized probe sites becomes comparable to target dimensions, whereas extents of DNA−DNA surface hybridization are instead consistent with limits imposed by buildup of surface (Donnan) potential. The two processes also fundamentally differ at high ionic strength, under conditions when electrostatic effects are weak. Here, variations in probe coverage have a much diminished impact on MO−DNA than on DNA−DNA hybridization for similarly crowded surface conditions. These various observations agree with a structural model of MO monolayers in which MO−DNA duplexes segregate to the buffer interface while unhybridized probes localize near the solid support. A general perspective is presented on using uncharged DNA analogues, which also include compounds such as peptide nucleic acids (PNA), in surface hybridization applications.

1. Introduction

Morpholinos (MOs) are synthetic nucleic acid mimics incorporating conventional DNA bases arranged along an uncharged backbone of morpholine rings connected by phosphorodiamidate groups.[1,2] The uncharged nature of MOs is anticipated to strongly impact the rules that underpin their diagnostic applications based on solid-phase hybridization.[3−6] In these applications, as encountered in microarray[7] and biosensor technologies,[8,9] analyte nucleic acid sequences from solution hybridize with complementary, immobilized strands ("probes") at a solid−liquid interface. In the crowded interfacial environment, hybridization is subject to a complex convergence of interactions whose elucidation is crucial to its optimization for applications.[10−23] This study presents an initial analysis of these interactions for the situation of MO probes hybridizing with DNA sequences from solution. Compared to other ana-

[†] Seventh Sense Biosystems Inc.
[‡] Polytechnic Institute of New York University.
[§] Columbia University.

(1) Summerton, J.; Weller, D. *Antisense Nucleic Acids* **1997**, *7*, 187.
(2) Summerton, J. E. *Lett. Pept. Sci.* **2004**, *10*, 215.
(3) Tercero, N.; Wang, K.; Gong, P.; Levicky, R. *J. Am. Chem. Soc.* **2009**, *131*, 4953.
(4) Gao, Z.; Ting, B. P. *Analyst* **2009**, *134*, 952.
(5) Wang, X.; Smirnov, S. *ACS Nano* **2009**, *3*, 1004.
(6) Zhang, G. J.; Luo, Z. H.; Huang, M. J.; Tay, G. K.; Lim, E. J. *Biosens. Bioelectron.* **2010**, doi:10.1016/j.bios.2010.04.001.
(7) Müller, H.-J.; Röder, T. *Microarrays*; Elsevier Academic Press: Burlington, MA, 2006.
(8) Vercoutere, W.; Akeson, M. *Curr. Opin. Chem. Biol.* **2002**, *6*, 816.
(9) Sassolas, A.; Leca-Bouvier, B. D.; Blum, L. J. *Chem. Rev.* **2008**, *108*, 109.
(10) Levicky, R.; Horgan, A. *Trends Biotechnol.* **2005**, *23*, 143.
(11) Peterson, A. W.; Heaton, R. J.; Georgiadis, R. M. *Nucleic Acids Res.* **2001**, *29*, 5163.
(12) Henry, M. R.; Stevens, P. W.; Sun, J.; Kelso, D. M. *Anal. Biochem.* **1999**, *276*, 204.
(13) Stevens, P. W.; Henry, M. R.; Kelso, D. M. *Nucleic Acids Res.* **1999**, *27*, 1719.
(14) Peterson, A. W.; Wolf, L. K.; Georgiadis, R. M. *J. Am. Chem. Soc.* **2002**, *124*, 14601.
(15) Sekar, M. M. A.; Bloch, W.; St John, P. M. *Nucleic Acids Res.* **2005**, *33*, 366.
(16) Su, H.-J.; Surrey, S.; McKenzie, S. E.; Fortina, P.; Graves, D. J. *Electrophoresis* **2002**, *23*, 1551.
(17) Yu, F.; Yao, D.; Knoll, W. *Nucleic Acids Res.* **2004**, *32*, e75.
(18) Fiche, J. B.; Buhot, A.; Calemczuk, R.; Livache, T. *Biophys. J.* **2007**, *92*, 935.
(19) Glazer, M.; Fidanza, J. A.; McGall, G. H.; Trulson, M. O.; Forman, J. E.; Suseno, A.; Frank, C. W. *Anal. Biochem.* **2006**, *358*, 225.
(20) Wong, E. L. S.; Chow, E.; Gooding, J. J. *Langmuir* **2005**, *21*, 6957.
(21) Lee, C. Y.; Harbers, G. M.; Grainger, D. W.; Gamble, L. J.; Castner, D. G. *J. Am. Chem. Soc.* **2007**, *129*, 9429.
(22) Lee, C. Y.; Nguyen, P. C. T.; Grainger, D. W.; Gamble, L. J.; Castner, D. G. *Anal. Chem.* **2007**, *79*, 4390.
(23) Xu, J.; Craig, S. L. *J. Am. Chem. Soc.* **2005**, *127*, 13227.

Table 1. Sequences and Purpose of Morpholino and DNA Molecules

abbreviation	sequence	comments
PM-F	5′ FcCA-NH-TTT TAA ATT CTG CAA GTG AT-CO$(CH_2)_3SS(CH_2)_3CONH_2$ 3′	20mer FcCA-labeled morpholino probe for surface hybridization
TD-F	5′ FEM-S-CAC TTG CAG AAT TTA AAA 3′	18mer FEM-labeled DNA target complementary to PM-F; used for surface hybridization
PM	5′ TTT TAA ATT CTG CAA GTG AT 3′	20mer unmodified morpholino for melting studies; same sequence as that of PM-F
PD	5′ TTT TAA ATT CTG CAA GTG AT 3′	20mer unmodified DNA for melting studies; same sequence as that of PM-F
TD	5′ CAC TTG CAG AAT TTA AAA 3′	18mer unmodified DNA for melting studies complementary to PM and PD; same sequence as that of TD-F

logues, such as peptide nucleic acids (PNAs),[24] MOs have few constraints on sequence composition or length and thus provide essential flexibility for applications in gene expression and pathogen identification which often employ lengths of up to 70 nt.[25,26]

The analysis of MO−DNA surface hybridization is presented, in part, by contrasting it with behavior of the corresponding DNA−DNA system in which the probe is instead a DNA molecule, as well as with related information available for PNA probes.[27−34] These cross-comparisons help form a consistent picture of why certain differences or similarities arise based on the type of probe used. After introducing main features of MO−DNA solution hybridization in section 3.1, we focus on hybridization on solid supports under high (section 3.2.2) and low (section 3.2.3) ionic strengths corresponding, respectively, to suppression and dominance of electrostatic control. The characteristic trends for MO−DNA surface hybridization, and their relationship to those observed with other probe types, are discussed in the context of the molecular organization of the hybridizing layers.

2. Materials and Methods

2.1. Oligonucleotides. Table 1 lists the abbreviations, sequences, and experimental purpose of the oligomers used. Morpholino probes, purified by precipitation, were purchased from Gene Tools LLC (Philomath, OR, U.S.A.). All surface hybridization measurements used the 20mer MO probe sequence PM-F and complementary 18mer DNA targets TD-F. The first two residues on the 3′ end of the probes serve as short spacers when tethered to a surface (Supporting Information, Figure S1.B). The other materials in Table 1 were used for solution melting measurements. Modification of PM-F probes and TD-F targets with the electroactive tags ferrocenecarboxylic acid−NHS ester (FcCA−NHS) and *N*-(2-ferroceneethyl)maleimide (FEM), respectively, is detailed in the Supporting Information. The distinct redox potentials of these two tags enabled simultaneous determination of probe and target surface coverages using cyclic voltammetry (CV),[3] as described in the Supporting Information.

2.2. Measurement and Analysis of Solution Melting Curves. All solution melting studies were performed in sodium phosphate buffers at pH 7.0, with no other salt present. Buffers were prepared by mixing mono- and dibasic sodium phosphate in the appropriate ratio to yield pH 7.0 at room temperature (approximately 22 °C). Throughout this study, buffer molarity refers to phosphate species; the actual concentration of sodium cations is approximately 1.6 times that of the phosphate. Given the low temperature coefficient of phosphate buffer, −0.0028 pH °C $^{-1}$, the maximal pH change during melting experiments was about −0.15 pH units; this modest variation was not corrected for and is not expected to be of consequence. Melting curves were measured using MO and DNA oligonucleotides of sequences identical to those used for surface hybridization but without end modifications (Table 1). MO−DNA and DNA−DNA (for comparison) melting curves were measured at 260 nm using a temperature ramp of 0.2 °C min^{-1}. Stoppered 1.4 mL quartz cuvettes (Starna Cells, Atascadero, CA, U.S.A.) were filled with pH 7.0 sodium phosphate buffer with the final concentration of both strands at 0.5 μmol L^{-1} as calculated from manufacturer-provided extinction coefficients. Measurements were performed at various buffer molarities, ranging from 0 to 1 mol L^{-1}, on a Cary 50 spectrometer equipped with a single-cuvette temperature-control Peltier stage (Quantum Northwest, Liberty Lake, WA, USA). Two complete heat−cool cycles were performed to ensure reversibility of the melting data. Examples of melting cycles and a description of the analysis used to extract thermodynamic parameters (ΔG^o, ΔH^o, ΔS^o) of solution hybridization are provided in the Supporting Information.

2.3. Preparation of Morpholino Probe Films. A 1.6 mm diameter disk polycrystalline gold working electrode (Bioanalytical Systems, West Lafayette, IN, U.S.A.) was first mechanically polished followed by electrochemical etching in a sulfuric acid/KCl solution as previously described.[35,36] The surface roughness factor r (r = true area/geometric area; $r \geq 1$) was measured from the double layer capacitance[35] and ranged from 1.32 to 1.82, with an average of 1.62 ± 0.15. All reported probe and target coverages have been corrected for the roughness of that particular surface. PM-F MO probes were immobilized to thus cleaned and characterized supports through their 3′ disulfide, using a fixed deposition time of 30 min and concentrations from 0.03 to 5 μmol L^{-1} in deionized (18.2 MΩ cm) water. Following probe deposition, supports were immersed for 150 min in 1 mmol L^{-1} mercaptopropanol (MCP) in deionized water to block chemisorptive interactions of the gold surface with nucleic bases. MCP assembles into a monolayer underneath the MO probes, leaving the probes attached through their thiolate−gold bond.[3] All transfer steps were ac-

(24) Egholm, M.; Buchardt, O.; Christensen, L.; Behrens, C.; Freler, S. M.; Driver, D. A.; Berg, R. H.; Kim, S. K.; Norden, B.; Nielsen, P. E. *Nature* **1993**, *365*, 566.
(25) Hughes, T. R.; et al. *Nat. Biotechnol.* **2001**, *19*, 342.
(26) Bodrossy, L.; Sessitsch, A. *Curr. Opin. Microbiol.* **2004**, *7*, 245.
(27) Jensen, K. K.; Orum, H.; Nielsen, P. E.; Norden, B. *Biochemistry* **1997**, *36*, 5072.
(28) Wang, J.; Palecek, E.; Nielsen, P. E.; Rivas, G.; Cai, X.; Shiraishi, H.; Dontha, N.; Luo, D.; Farias, P. A. M. *J. Am. Chem. Soc.* **1996**, *118*, 7667.
(29) Wang, J.; Rivas, G.; Cai, X. H.; Chicharro, M.; Parrado, C.; Dontha, N.; Begleiter, A.; Mowat, M.; Palecek, E.; Nielsen, P. E. *Anal. Chim. Acta* **1997**, *344*, 111.
(30) Liu, J. Y.; Tiefenauer, L.; Tian, S. J.; Nielsen, P. E.; Knoll, W. *Anal. Chem.* **2006**, *78*, 470.
(31) Park, H.; Germini, A.; Sforza, S.; Corradini, R.; Marchelli, R.; Knoll, W. *Biointerphases* **2007**, *2*, 80.
(32) Kambhampati, D.; Nielsen, P. E.; Knoll, W. *Biosens. Bioelectron.* **2001**, *16*, 1109.
(33) Ananthanawat, C.; Vilaivan, T.; Hoven, V. P.; Su, X. D. *Biosens. Bioelectron.* **2010**, *25*, 1064.
(34) Sato, Y.; Fujimoto, K.; Kawaguchi, H. *Colloids Surf., B* **2003**, *27*, 23.
(35) Oesch, U.; Janata, J. *Electrochim. Acta* **1983**, *28*, 1237.
(36) Shen, G.; Tercero, N.; Gaspar, M. A.; Varughese, B.; Shepard, K.; Levicky, R. *J. Am. Chem. Soc.* **2006**, *128*, 8427.

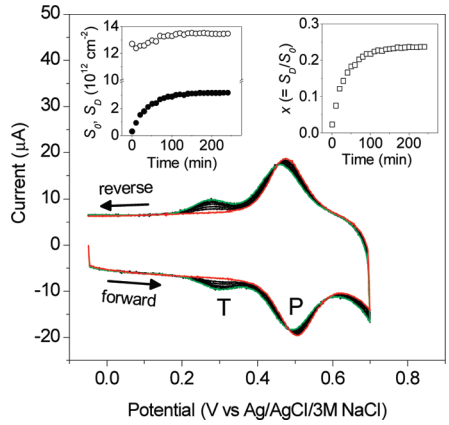

Figure 1. (Main panel) Time series of CV voltammograms, shown for $S_0 = 1.3 \times 10^{13}$ cm^{-2} and $C_B = 0.11$ mol L^{-1}. The $t = 0$ trace (—), in red, corresponds to the start of hybridization. The last trace, at $t = 240$ min, is plotted in green (—). Voltammograms were measured at 10-min intervals at 20 V s^{-1}, between −0.05 and 0.7 V. Insets show the probe and target coverages, S_0 (○) and S_D (●), and the conversion $x = S_D/S_0$ (□) determined from integrated areas of the probe "P" and target "T" peaks.

complished with the electrode covered by a droplet of solution to prevent possible contamination through ambient contact.

2.4. Surface Hybridization Assays. Hybridizations were performed at 22 ± 1 °C in pH 7.0 phosphate buffer, with no other salt present, using a target concentration of 10 nmol L^{-1} under continuous stirring. This quantity of target represents a 50-fold or higher excess over that required to fully hybridize the probe layers; therefore, the target concentration is expected to remain nearly constant during an assay. Hybridization was followed for 47 different combinations of total probe coverage S_0 and buffer molarity C_B, where C_B represents the total phosphate molarity (predominantly $H_2PO_4^-$ and HPO_4^{2-} species). The experimental conditions ranged from 1×10^{12} to 2.5×10^{13} cm^{-2} in probe coverage, and included C_B settings of 1.0, 0.33, 0.11, 0.037, and 0.012 mol L^{-1}. Each hybridization used a freshly prepared probe layer to ensure a similar initial state.

During hybridization the surface potential was held at 0 V, where all potentials are reported relative to an Ag/AgCl/3 mol L^{-1} NaCl reference electrode (Bioanalytical Systems, West Lafayette, IN, U.S.A.). The reference electrode was placed in a double liquid junction to minimize diffusion of NaCl from its reservoir into the hybridization buffer. A platinum wire served as the counter electrode. A hybridization run was initiated by placing a freshly prepared PM-F probe film for 5 min in target-free buffer, after which a CV trace was measured to determine the starting probe coverage from FcCA redox current. Next, FEM-labeled TD-F target was added to a concentration of 10 nmol L^{-1}, and the progress of hybridization was monitored by collecting CV traces 10 min apart. CV measurements were performed at 20 V s^{-1} between −0.05 and 0.7 V, requiring 0.08 s to complete per scan. At the conclusion of a CV scan the surface potential was returned to and maintained at 0 V until the next measurement. The total time per hybridization, from time $t = 0$ when target was first added to time of measurement of the last CV trace, was 4 h.

Figure 1 presents an example of a CV time series. The forward leg of the $t = 0$ CV trace shows the probe FcCA peak (labeled "P") around 0.5 V, the potential at which the tag undergoes reversible oxidation by giving up an electron according to FcCA → $FcCA^+ + e^-$. On the reverse half-scan $FcCA^+$ is reduced back to its initial FcCA state at around 0.47 V. As hybridization progresses, the target FEM peak (labeled "T") appears at around 0.28 V and increases in area, while the probe peak remains approximately constant. The modest shift in the probe peak's position to lower potentials is attributed to onset of a membrane

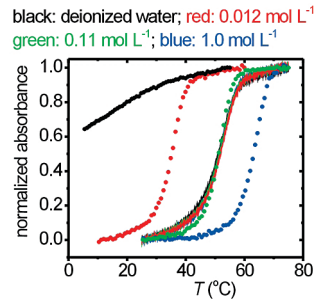

Figure 2. Effect of buffer concentration on MO−DNA (lines) and DNA−DNA (points) melting. PM morpholino or PD DNA probes were hybridized in a 1:1 stoichiometry to TD targets. Melting curves have been normalized to span from 0 to 1. Conditions: pH 7.0 sodium phosphate buffer; 1.0 μmol L^{-1} total strand concentration; 0.2 °C min^{-1} temperature ramp; second cooling cycle. In all cases, reversibility was confirmed by superposition of heating and cooling cycles (Figure S2.A in Supporting Information).

potential,[37−39] brought on by the growing charge density of the MO layer from binding of target strands. Linear scaling of the peak current with the scan rate confirmed that the signals originated from surface-immobilized tags[40] (i.e., hybridized targets) and not from diffusing species in solution.

The FcCA and FEM signals from CV traces were used to determine the total probe S_0 and target S_D coverages, Figure 1 left inset, as described previously;[3] an example of such a fit is provided in the Supporting Information. The apparent ∼5% increase in S_0 with time is attributed to bias of the computer algorithm used for CV analysis by variation in the experimental baseline as hybridization proceeds, not to an actual change in probe coverage.

3. Results and Discussion

3.1. MO−DNA Solution Hybridization. MO−DNA hybridization in solution was insensitive to phosphate buffer molarity C_B from 0 (deionized water) to 1.0 mol L^{-1}. The MO−DNA melting curves superposed with C_B in this entire range of ionic strength, as shown by the solid lines in Figure 2. In contrast, DNA−DNA melting transitions were destabilized as C_B decreased, with a shift of the melting temperature T_M to lower values. The well-known dependence of T_M on C_B, for DNA−DNA hybridization, can be interpreted as arising from reorganization of small ions to mitigate the duplex electrostatic energy (e.g., through counterion condensation[41]). Since the high charge density of duplex DNA attracts more counterions than the sum total of two single strands, duplex formation is favored by the higher availability of counterions (i.e., high C_B) which decreases the entropic penalty for the additional association. Following similar reasoning, the insensitivity of MO−DNA melting to C_B suggests that the counterion reorganization as a result of hybridization is minimal. Interpreted in the context of counterion condensation, the lack of C_B dependence implies that the number of condensed counterions is not significantly altered by hybridization.

Thermodynamic parameters derived from analysis of melting curves are listed in Table 2. The energetic change from molecular interactions, as reflected in ΔH^o, is seen to be less

(37) Donnan, F. G. *J. Membr. Sci.* **1995**, *100*, 45.
(38) Naegeli, R.; Redepenning, J.; Anson, F. C. *J. Phys. Chem.* **1986**, *90*, 6227.
(39) Wang, K.; Zangmeister, R. A.; Levicky, R. *J. Am. Chem. Soc.* **2009**, *131*, 318.
(40) Laviron, E. *J. Electroanal. Chem.* **1979**, *101*, 19.
(41) Manning, G. S. *Q. Rev. Biophys.* **1978**, *11*, 179.

Table 2. Thermodynamic Parameters of Solution Hybridization[a,b]

	MO−DNA			DNA−DNA		
C_B mol/L	ΔH^o kcal/mol	ΔS^o kcal/(mol K)	ΔG^o kcal/mol	ΔH^o kcal/mol	ΔS^o kcal/(mol K)	ΔG^o kcal/mol
1.0	−115	−0.323	−14.8	−131	−0.358	−20.0
0.11	−115	−0.324	−14.5	−137 (−137)	−0.391 (−0.390)	−15.7 (−15.9)
0.012	−118	−0.333	−14.7	−130 (−137)	−0.390 (−0.405)	−9.0 (−11.3)
0.0	−113	−0.317	−14.7	−	−	−

[a] All entries were calculated from melting curves as described in the Supporting Information, except for values in parentheses which are predictions from UNAFold.[42,43] [b] ΔG^o is at 37 °C; ΔH^o and ΔS^o are assumed to be temperature independent.

favorable for MO−DNA than for DNA−DNA hybridization by about 20 kcal mol^{-1}, corresponding to ∼14% difference. This suggests the molecular fit between a DNA and a complementary MO strand is not as efficient in accommodating local interactions as that between two DNA strands. The lower enthalpic change for MO−DNA melting manifests in broader melting transitions than for same-sequence DNA−DNA (Figure 2). In addition, the broader transitions may reflect a greater dispersion in molecular interactions due to the chiral P centers in the MO backbone (Figure S1.A, Supporting Information), since variations in stereochemical configuration of these groups from strand to strand may perturb hybrid stability. From Table 2, the entropic costs of hybridization, as represented by ΔS^o, increase for DNA−DNA hybridization at lower C_B while those for MO−DNA hybridization are unaffected. This is consistent with above explanation in terms of counterion condensation effects. As a consequence of the increased entropic penalty for DNA−DNA hybridization as C_B decreases, the overall free energy ΔG^o begins to favor the MO−DNA reaction below $C_B \approx 0.1$ mol L^{-1}.

The experimental values for DNA−DNA hybridization can be compared to predictions from UNAFold,[42,43] shown in parentheses in Table 2. Good agreement is observed between measured and calculated values at $C_B = 0.11$ mol L^{-1}, but the agreement worsens for 0.012 mol L^{-1} where the prediction algorithm is near its limit. Based on the decreased experimental ΔH^o and ΔS^o under these conditions, and the ultimate denaturation of the DNA−DNA duplex in deionized water (Figure 2), the DNA−DNA hybrids are suspected to be no longer fully formed at 0.012 mol L^{-1}; thus, the two-state assumption of the theory is not satisfied. For $C_B = 1.0$ mol L^{-1}, the corresponding Na^+ concentration of 1.6 mol L^{-1} exceeded the allowed upper predictive limit; therefore, no comparison was made for this buffer molarity.

PNA−DNA hybridization in solution[44,45] bears both similarities and differences to the MO−DNA system. Based on 10mer and 15mer sequences investigated by Tomac et al.,[44] the PNA−DNA system is similar in that it also exhibits a less favorable enthalpy of hybridization than for DNA−DNA, leading to broadened melting transitions. As counterion concentration (i.e., C_B) decreases, PNA−DNA hybridization also becomes favored over DNA−DNA binding and this outcome is similarly attributed to entropic destabilization of DNA−DNA hybridization by greater costs of counterion association at low C_B. However, in part because its enthalpic deficit was less, PNA−DNA hybridization was favored over the corresponding DNA−DNA pair already at counterion concentrations of ∼1 mol L^{-1}, compared to ∼0.1 mol L^{-1} for the MO−DNA sequence of Table 2. Interestingly, and in contrast to MO−DNA hybridization, the PNA−DNA reaction exhibits a modest salt-dependence with hybridization being favored by low concentrations of counterions. This trend is attributed to a release, as opposed to condensation, of counterions upon hybridization.[44]

3.2. MO−DNA Surface Hybridization. 3.2.1. General Trends. This section compares MO−DNA and DNA−DNA surface hybridization under similar conditions of probe coverage and buffer molarity. The DNA−DNA data were recently analyzed in detail,[46] providing a starting point for discussion of the less understood MO−DNA system. The following contributions were identified as important to DNA−DNA surface hybridization: (1) a solution-like dependence on counterion concentration due to participation of counterions in the formation of double-stranded structures; (2) existence of a surface Donnan potential[37−39] V_S, defined between the interior of the probe layer and the external buffer environment, that penalizes entry of target molecules into the layer; (3) interactions experienced by probes in the crowded surface environment, such as association of complementary tracts among two or more probes, that compete with binding to target molecules; and (4) steric, or packing, limitations that set in at high coverages. MO−DNA surface hybridization may be anticipated to differ in at least two ways from these conclusions. Since, in solution, MO−DNA hybridization did not depend on counterion concentration, the first of the above effects is expected to be absent.[47] Second, since MO probes are not charged, only hybridized targets contribute to the repulsive surface potential, V_S.

Differences are also expected in the molecular organization of the probe films. *In situ* data on the structure of DNA monolayers[48] indicate that unhybridized probes largely occupy the same region of space as the duplexes, so that there is little stratification normal to the surface. In contrast, a recent theoretical analysis of capacitance measurements on MO monolayers found good agreement when unhybridized MO probes were treated as a desolvated, collapsed layer.[3] A collapsed organization is also consistent with the approximately millimolar aqueous solubility of MO probes. Since this solubility limit is exceeded by a factor of 10 or more for a surface-tethered layer, MO probes are expected to primarily exist as a precipitated film rather than well-solvated chains. However, when an MO probe hybridizes to a DNA target, the resultant duplex acquires charge; thus, MO−DNA duplexes are expected to be more soluble than unhybridized MO probes. These considerations

(42) Markham, N. R.; Zuker, M. *Nucleic Acids Res.* **2005**, *33*, W577.
(43) Markham, N. R.; Zuker, M. In *Bioinformatics: Volume II: Structure, Function and Applications*; Keith, J. M., Ed.; Methods in Molecular Biology, Vol. 453, Humana Press: Totowa, NJ, 2008; p 3.
(44) Tomac, S.; Sarkar, S.; Ratilainen, T.; Wittung, P.; Nielsen, P. E.; Nordén, B.; Gräslund, A. *J. Am. Chem. Soc.* **1996**, *118*, 5544.
(45) Ratilainen, T.; Holmn, A.; Tuite, E.; Nielsen, P. E.; Nordén, B. *Biochemistry* **2000**, *39*, 7781.
(46) Irving, D.; Gong, P.; Levicky, R. *J. Phys. Chem. B* **2010**, *114*, 7631.
(47) The structure of MO−DNA duplexes in solution and on surfaces is assumed to be the same.
(48) Levicky, R.; Herne, T. M.; Tarlov, M. J.; Satija, S. K. *J. Am. Chem. Soc.* **1998**, *120*, 9787.

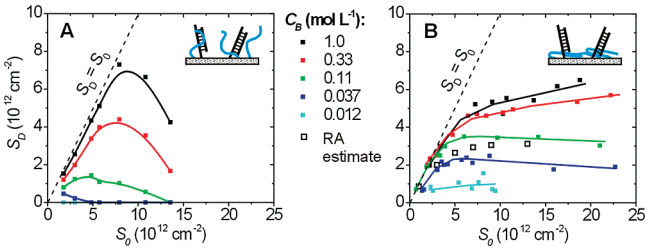

Figure 3. Surface coverage S_D of probe−target duplexes as a function of total probe coverage, S_0, and buffer concentration, C_B. (A) DNA probes; 100 nmol L^{-1} target concentration; 2 h hybridization time.[49] (B) Morpholino probes; 10 nmol L^{-1} target concentration; 4 h hybridization time. "RA estimate" in (B) is taken from a random adsorption simulation reported in reference 50 (see text for discussion). Schematic drawings in the insets illustrate expected organization of the films.

indicate that the most likely arrangement of a partially hybridized MO film is one in which MO−DNA duplexes segregate to the interface with the buffer, while unhybridized probes remain near the solid support. The insets in A and B of Figure 3 provide a schematic depiction of the expected organization of partially hybridized DNA and MO films, respectively. In anticipation of later discussion we also note that, since PNA probes are even less soluble than morpholinos, PNA monolayers would similarly be expected to consist of less-solvated unhybridized probes near the solid support while PNA−DNA hybrids segregate to the buffer interface.

The main frames in A and B of Figure 3 summarize the surface hybridization data. In these plots, coverage S_D of probe−target duplexes for DNA−DNA (Figure 3A) and MO−DNA (Figure 3B) systems is shown as a function of the total probe coverage, S_0, and buffer molarity, C_B. S_0 is the sum of unhybridized and hybridized probes; that is, $S_0 = S_P + S_D$ where S_P is the remaining coverage of unhybridized probes. In all cases S_D appeared to reach a stationary state as in Figure 1. The DNA−DNA data are from an earlier study[49] that used 20mer probes of the same sequence as that of PM-F, with hybridization also performed to complementary FEM-labeled 18mer targets. The DNA−DNA experiments differed in that labeling of targets was at the 3′ end, the targets were complementary to the 18 base positions on the probe closer to the solid support, and a 10-fold higher target concentration (100 nmol L^{-1}) was used. As seen in Figure 3, both sets of experiments produced comparable extents of hybridization over similar ranges of S_0 and C_B.

The dashed lines in A and B of Figure 3 correspond to full hybridization, $S_D = S_0$. This saturation limit is approached for both DNA−DNA and MO−DNA hybridization under favorable conditions, namely high C_B and low S_0. High C_B favors hybridization by diminishing the electrostatic cost $z_T e V_S$ (where z_T is the signed target valency and e is the elementary charge) of target partitioning from solution into the layer, while lower S_0 favors hybridization by decreasing penalties from steric crowding and from any probe−probe interactions that may compete with target binding. For DNA probes, lower S_0 also diminishes V_S since it decreases the quantity of immobilized surface charge.

Differences between DNA−DNA and MO−DNA surface hybridization, discussed below, can be identified from the manner in which the two types of probe respond to variations in C_B and S_0 away from the $S_D = S_0$ saturation limit. For MO−DNA two behaviors emerge, Figure 3B. For C_B of 0.11 mol L^{-1} and lower, the data exhibit strong dependence on buffer molarity. For the 0.33 and 1 mol L^{-1} curves, sensitivity to C_B is suppressed. The following sections focus on these situations of strong and weak charge effects, respectively. In each case, existing understanding of the DNA−DNA system will be also summarized as background for discussing MO−DNA surface hybridization.

3.2.2. MO−DNA Surface Hybridization under Weak Electrostatics ($C_B \geq 0.33$ mol L^{-1}). For the highest buffer molarities of 0.33 and 1 mol L^{-1}, DNA−DNA hybridization (Figure 3A) is characterized by a nonmonotonic dependence of S_D on S_0, with a maximum in S_D at intermediate probe coverage,[49,51−53] combined with significant dependence on buffer molarity. The sharpness of the decrease in S_D at high S_0, past the maximum, has been attributed to onset of constraints from molecular packing (i.e., contact interactions) based on additional evidence from isotherm measurements.[46] The C_B-dependence arises both from participation of counterions in formation of double-stranded structure, analogous to salt-dependence of solution hybridization, and from the repulsive surface potential V_S, arising from presence of immobilized DNA charge which penalizes entry of like-charged targets into the layer.

In comparison, for the same conditions of $C_B = 0.33$ and 1 mol L^{-1}, MO−DNA surface hybridization is only weakly dependent on C_B, Figure 3B. This relative unimportance of electrostatics is attributed to neutrality of MO probes, which therefore do not contribute to V_S and in this way lower the electrostatic penalty for target entry, and to independence of MO−DNA duplex formation on counterion concentration, as discussed in section 3.1. With electrostatics of secondary importance, the suppression of hybridization seen beyond $S_0 \approx 5 \times 10^{12}$ cm^{-2} must be predominantly attributed to nonelectrostatic constraints arising from molecular packing and contact interactions.

At the simplest level, hybridization under crowded conditions must recognize that, as S_0 increases, a growing fraction of probes will find themselves next to one or more neighbors at distances less than a duplex diameter. This proximity will make it impossible for a perfect duplex to form at each probe site, and must therefore lower activity of the probes. The fraction of sites not affected by such "duplex overlap" constraints, i.e. separated by a distance equal to at least one duplex diameter from other duplexes, was estimated by Hagan and Chakraborty (HC) for DNA−DNA duplexes as a function of S_0 using a random adsorption (RA) simulation.[50] A hard core duplex diameter of 3.2 nm, rather than the 2 nm corresponding to molecular dimensions, was used to also account for hydration repulsions[54,55] as part of the hard core contact exclusion. The predictions of HC, assuming that maximum hybridization is reached, are reproduced as the open squares in Figure 3B. The functional relationship from the simulation is in good agreement with our high C_B data, although it underestimates S_D by about a factor

(49) Gong, P.; Levicky, R. *Proc. Natl. Acad. Sci. U.S.A.* **2008**, *105*, 5301.
(50) Hagan, M. F.; Chakraborty, A. K. *J. Chem. Phys.* **2004**, *120*, 4958.
(51) Gong, P.; Lee, C.-Y.; Gamble, L. J.; Castner, D. G.; Grainger, D. W. *Anal. Chem.* **2006**, *78*, 3326.
(52) Shen, G.; Anand, M. F. G.; Levicky, R. *Nucleic Acids Res.* **2004**, *32*, 5973.
(53) Steel, A. B.; Herne, T. M.; Tarlov, M. J. *Anal. Chem.* **1998**, *70*, 4670.
(54) Strey, H. H.; Parsegian, V. A.; Podgornik, R. *Phys. Rev. Lett.* **1997**, *78*, 895.
(55) Strey, H. H.; Parsegian, V. A.; Podgornik, R. *Phys. Rev. E* **1999**, *59*, 999.

of 2. This underestimate may reflect disallowance of partially formed or distorted duplexes in the simulation, which in the experimental system may circumvent the hard core interaction to a degree, and/or an overestimate of 3.2 nm as the diameter applicable to MO−DNA duplexes. Nevertheless, given the good qualitative agreement with allowance for uncertainties in duplex dimensions, a simple mechanism of duplex overlap appears to be a sufficient explanation for suppression of MO−DNA hybridization at high C_B.

In contrast, DNA−DNA hybridization experiences a sharp drop as S_0 increases (Figure 3A) which runs contrary to the MO−DNA trend. The pronounced decrease indicates that hybridization to DNA probes is subject to penalties that either do not apply to or are weaker for MO probes. The most readily suggested explanation is electrostatic penalties to target partitioning, which would be enhanced by an increase in coverage of charged DNA probes and therefore expected to suppress S_D, whereas this effect would be absent for neutral MO probes. However, such an explanation seems incomplete as electrostatic effects should weaken as C_B rises, yet the drop in S_D with S_0 does not noticeably lessen at high C_B. Therefore, electrostatic effects appear to be of secondary importance under these conditions, and the decrease in S_D with S_0 must be attributed to nonelectrostatic penalties. A further clue is that the penalties must be less significant for MO−DNA hybridization, for which the decrease in S_D with S_0 is not observed.

We postulate that the suppression of DNA−DNA hybridization at high C_B and high S_0 stems from nonelectrostatic, repulsive *probe−duplex* interactions. This hypothesis can explain our observations as follows. For MO films, unhybridized probes exist in a collapsed state and therefore are "out of the way"; thus, contact between duplexes and unhybridized probes is limited. The highest probe coverages, assuming completely desolvated MO films, correspond to less than a 2 nm thickness[56] so that contact would be expected only at the base of a duplex. Therefore, effects from probe−duplex interactions should be relatively modest. However, we must also be careful in that the nature of interactions between MO probes and MO−DNA duplexes is not known. If the interactions are not strongly repulsive it may not be necessary to invoke a collapsed organization for unhybridized MO probes, even though a collapsed organization is expected. Incidentally, the simulation results of reference[50] in Figure 3B accounted only for constraints due to duplex−duplex overlap. By neglecting probe-duplex interactions, the simulation therefore represents the correct comparison to MO−DNA hybridization, in the absence of interference from unhybridized probes.

In contrast, when DNA probes are used probe segments are distributed throughout the film. In this case, probe-duplex contacts will arise along the length of a duplex, and if the contacts are repulsive then formation of new duplexes will be destabilized at the multiple points of contact. The nature of probe−duplex interactions in hybridizing DNA monolayers has been discussed in the context of microcantilever experiments.[57−60] In such experiments, hybridization alters the forces acting between the DNA molecules, and these changes are quantified from deflection of the microcantilevers. A theoretical analysis of microcantilever data concluded that, at high salt concentration, the principal source of deflection was indeed of nonelectrostatic origin and instead originated from hydration repulsions.[61] Hydration repulsions stem from the disruption of the ordering of water around DNA chains when strands are forced into proximity[54,55] and are expected to be just as important whether hybridization is performed on a rigid support, as in the present study, or on a deformable microcantilever. On the basis of these considerations we tentatively attribute the sharp decrease in S_D, observed in the DNA−DNA data as S_0 increases for buffer molarity near 1 mol L^{-1}, to hydration repulsions between unhybridized probes and duplexes.

3.2.3. MO−DNA Surface Hybridization under Electrostatic Dominance ($C_B \leq 0.11$ mol L^{-1}). At lower buffer molarities, 0.11−0.012 mol L^{-1}, an increase in S_0 suppresses DNA−DNA hybridization to below detection, as in the 0.11 and 0.037 mol L^{-1} data in Figure 3A. At these lower molarities, ionic screening is weaker and the importance of electrostatic effects increases. Analysis of the DNA−DNA data using theoretical models of surface hybridization[62,63] in reference 46 indicates that these trends can be understood as primarily reflecting changes in the surface potential V_S, and hence target partitioning penalty ez_TV_S, as C_B and S_0 change. In comparison, MO−DNA surface hybridization, away from the $S_D = S_0$ limit, is also dependent on C_B but varies only weakly with S_0. The dependence on C_B contrasts with the insensitivity of solution hybridization to C_B (Figure 2), and is attributed to the surface-specific effect of previously hybridized targets presenting an electrostatically controlled barrier to those arriving later. The nature of this barrier is further considered below.

The trends in MO−DNA surface hybridization can be further compared to those obtained using PNA probes, which are similarly able to hybridize DNA targets at very low ionic strengths.[28,30,33] Interestingly, PNA−DNA surface hybridization is unusual in that the dependence on ionic strength is typically nonmonotonic, with hybridization maximized at intermediate ionic strengths of around 0.01 mol L^{-1},[28,29,31,33] as opposed to the monotonic increase in S_D with C_B observed for the MO−DNA data. Similar to the MO−DNA system, the decrease in PNA−DNA hybridization at low ionic strengths, below the maximum, can be attributed to onset of electrostatic suppression of hybridization due to repulsion of targets in solution by ones that have already bound.[31] We moreover propose that suppression above the maximum, at higher ionic strengths, may reflect decreased stability of PNA−DNA duplexes at higher salt as established independently from solution measurements.[31,44] This would explain why PNA−DNA surface hybridization exhibits a maximum with ionic strength while MO−DNA surface hybridization does not, since stability of MO−DNA duplexes is independent of ionic strength (Figure 2).

(56) The desolvated thickness d, in nanometers, is $d = S_P N_P v_{nt}/(1 - a_D S_D)$ where $N_P = 20$ is the number of residues per probe, $v_{nt} = 0.53$ nm^3 is the volume of one residue, $a_D = \pi$ nm^2 is the cross-sectional area of a duplex, and S_P and S_D are in units of nm^{-2}. v_{nt} and a_D are assumed to be the same as for DNA. The denominator is the fraction of surface available to the probes.

(57) Fritz, J.; Baller, M. K.; Lang, H. P.; Rothuizen, H.; Vettiger, P.; Meyer, E.; Guntherodt, H. J.; Gerber, C.; Gimzewski, J. K. *Science* **2000**, *288*, 316.
(58) McKendry, R.; Zhang, J.; Arntz, Y.; Strunz, T.; Hegner, M.; Lang, H. P.; Baller, M. K.; Certa, U.; Meyer, E.; Guntherodt, H.-J.; Gerber, C. *Proc. Natl. Acad. Sci. U.S.A.* **2002**, *99*, 9783.
(59) Wu, G.; Ji, H.; Hansen, K.; Thundat, T.; Datar, R.; Cote, R.; Hagan, M. F.; Chakraborty, A. K.; Majumdar, A. *Proc. Natl. Acad. Sci. U.S.A.* **2001**, *98*, 1560.
(60) Bergese, P.; Oliviero, G.; Alessandri, I.; Depero, L. E. *J. Colloid Interface Sci.* **2007**, *316*, 1017.
(61) Hagan, M. F.; Majumdar, A.; Chakraborty, A. K. *J. Phys. Chem. B* **2002**, *106*, 10163.
(62) Halperin, A.; Buhot, A.; Zhulina, E. B. *Biophys. J.* **2004**, *86*, 718.
(63) Vainrub, A.; Pettitt, B. M. *Phys. Rev. E* **2002**, *66*, 041905.

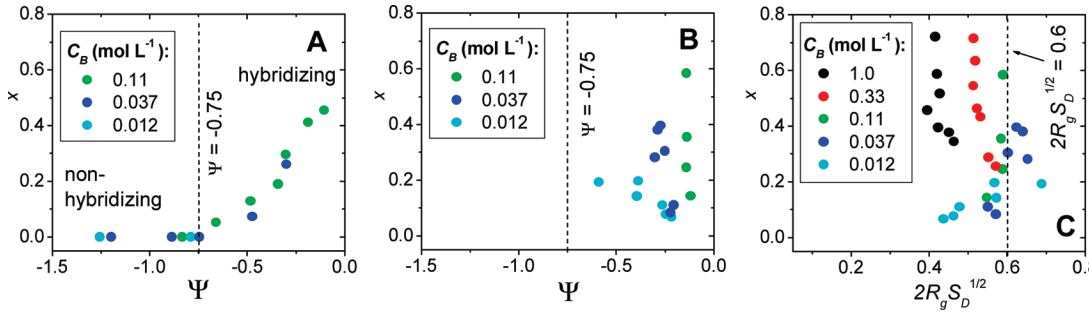

Figure 4. Plots of the hybridization conversion $x = S_D/S_0$ for (A) DNA−DNA hybridization parametrized by Ψ, (B) MO−DNA hybridization parametrized by Ψ, and (C) MO−DNA hybridization parametrized by the ratio of target size $2R_g$ to the separation between duplexes $S_D^{-1/2}$.

Because electrostatics can manifest through various mechanisms, the question arises whether their influence on DNA−DNA and MO−DNA hybridization is of the same origin. It will prove helpful to work with dimensionless quantities to constrain the number of possible relationships between hybridization extents and prospective electrostatic influences. A suitable dimensionless metric for the extent of hybridization is the conversion $x = S_D/S_0$ previously introduced in Figure 1. Since x is dimensionless, it can only depend on dimensionless combinations of other parameters; i.e. $x = f(G_1,G_2, ...)$, where f represents an unknown functional dependence and G_i are dimensionless groupings of parameters that govern hybridization. Assuming dominance of a single electrostatic effect characterized by a dimensionless group G_{el}, the relationship of interest simplifies to $x \approx f(G_{el})$.

To illustrate this approach, we first recast the conclusions of reference 46, which identified V_S as governing DNA−DNA surface hybridization at low buffer molarities, into the $x \approx f(G_{el})$ framework. A dimensionless surface potential Ψ follows from the requirement of electrochemical equilibria,[37,46]

$$\Psi = eV_S/kT = \frac{1}{z_j}\ln\left(\frac{C_{j,B}}{C_{j,S}}\right)$$

where j is an ionic species that partitions between solution and the probe layer, e is the elementary charge, k is the Boltzmann constant, T is temperature, z_j is the signed valence of j, and $C_{j,B}/C_{j,S}$ is the equilibrium ratio of the concentration of j in solution to that at the surface, inside the hybridizing layer. $C_{j,S}$ depends on the amount of immobilized strand charge and is calculated as in reference 46 with modifications, in the case of MO probes, for lack of probe charge and a collapsed organization of unhybridized probes (Supporting Information).

Figure 4 plots x against Ψ for the DNA−DNA (Figure 4A) and MO−DNA (Figure 4B) scenarios. Only those experimental points clearly falling under condition of suppressed hybridization were used, so that hybridization was limited by electrostatics rather than scarcity of probe sites. For DNA−DNA hybridization, Figure 4A, the collapse of data from various combinations of C_B and S_0 confirms that Ψ effectively summarizes the principal impact of electrostatics on hybridization.[64] It can be further confirmed that, for all the plotted points, the partitioning penalty $z_T\Psi kT$ for a target to enter the probe layer is comparable to or exceeds kT; therefore, the surface potential is indeed expected to significantly influence hybridization. The dashed vertical line in Figure 4A separates hybridizing from nonhybridizing conditions, with the threshold corresponding to $\Psi \approx -0.75$.

For MO−DNA hybridization, Ψ originates solely from charge brought to the surface by hybridized targets. The expectation is that hybridization should progress to an equilibrium at which Ψ has built up sufficiently to make the overall energetics unfavorable. This, however, is not what is observed. Rather, from Figure 4B it is evident that Ψ does not correlate well with x. Together, these observations cast doubt on the surface potential as the governing factor for our MO−DNA hybridization data.

The inadequacy of Ψ may derive from lateral nonuniformity of the layers. While a DNA probe film contains, in addition to duplexes, charged probes with flexible backbones that can more uniformly distribute their charge over the solid support, in MO layers only the duplexes are charged which, under the investigated conditions, are separated by distances corresponding to one to two duplex lengths, or 6−12 nm. This degree of coverage may not be sufficient to provide the lateral uniformity required to establish a well-defined surface potential; therefore, at the realized extents of hybridization, Ψ may not yet be a useful parameter.

Alternately, other dimensionless groups G_{el} may be more suitable than Ψ for correlating x. Such groups would need to include information other than that in Ψ on how electrostatics influence MO−DNA surface hybridization. Returning to the earlier discussion of the organization of MO monolayers, if the MO probes are collapsed, then a target from solution would have to first penetrate through the MO−DNA duplex layer before it could hybridize. The rate of traversal is expected to depend on the ratio of target size, which depends on buffer molarity and hence is an "electrostatic" quantity, to the available separation between duplexes. Target size can be estimated from the radius of gyration R_g, while the separation between duplexes is proportional to $S_D^{-1/2}$; therefore, a suitable dimensionless group is $2R_gS_D^{1/2}$ (the factor of 2 is included to more accurately represent target size through the diameter $2R_g$). The expectation is that targets should readily penetrate the duplex layer as long as $2R_gS_D^{1/2} < 1$, Figure 5. $R_g = (l_PL/3)^{1/2}$ can be estimated from the target contour length $L = N_T\, l_N$ with $N_T = 18$ the number of nucleotides and $l_N = 0.43$ nm the length per nucleotide,[65] and the salt-dependent persistence length of single-stranded

(64) In reference 49 a dimensionless group $\Pi = C_P/C_{Na^+,B}$ was defined to delineate conditions for onset of significant hybridization, where C_P is the concentration of immobilized charge from the DNA probes and $C_{Na^+,B}$ is concentration of sodium cations in solution. Π is related to the $C_{j,B}/C_{j,S}$ ratio (written for Na^+) in the definition for Ψ by taking the limit to dilute $C_{Na^+,B}$ (i.e. to nonhybridizing conditions) since, for a nearly electroneutral probe layer, $C_{Na^+,S}$ then approaches C_P.

(65) Record, M. T.; Anderson, C. F.; Lohman, T. M. *Q. Rev. Biophys.* **1978**, *11*, 103.

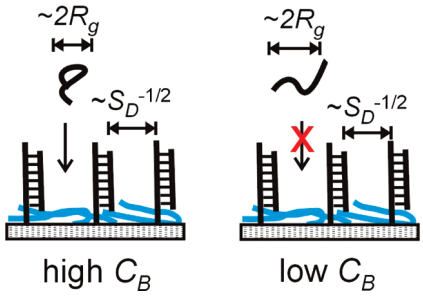

Figure 5. Target molecules are expected to more easily enter a duplex layer when their dimensions are smaller than the separation between duplexes, $2R_g < S_D^{-1/2}$. Because of electrostatic swelling of the target strands at low ionic strength, as C_B decreases, their entry is expected to be increasingly hindered.

DNA $l_P = a_0 + a_1/C_{Na,B}^{1/2}$ where a_0 and a_1 were reported in Tinland et al.[66]

Figure 4C shows the resultant plot of x against $2R_gS_D^{1/2}$. Although the 0.012 mol L^{-1} data suffer from extensive scatter, which stems from difficulties with deconvoluting rather small target signals from much larger probe peaks in the electrochemical data, we can nevertheless see that for the lower buffer molarities ($C_B \leq 0.11$ mol L^{-1}) hybridization progressed to a duplex coverage S_D such that $2R_gS_D^{1/2} \approx 0.6$. This limit is consistent with the notion of hindered target transport across the duplex layer when spacing between duplexes becomes comparable to target size, i.e. when $2R_gS_D^{1/2} \approx 1$. Figure 4C also shows that $2R_gS_D^{1/2}$ correlates the data significantly better than Ψ, with the three lowest buffer molarities approximately aligning. For comparison, the 0.33 and 1 mol L^{-1} data are also plotted in Figure 4C. These higher buffer molarities exhibit systematic deviations toward lower $2R_gS_D^{1/2}$, indicating that hybridization should be less limited by target transport across the duplex layer under these conditions (except perhaps for the last two points at 0.33 mol L^{-1}, which correspond to the highest two duplex coverages for this C_B in Figure 3B).

Target transport across the MO−DNA duplex layer represents a kinetic barrier; therefore, the results in Figure 4C suggest that, for $C_B \leq 0.11$ mol L^{-1}, hybridized coverages are constrained by *kinetic* limitations and that equilibrium was not realized. Rather, these results imply that as hybridization progresses the barrier to target penetration across the duplex layer increases, with the consequence that kinetics slow down sufficiently to appear to stop over our experimental time scales. A somewhat analogous situation was previously realized for DNA−DNA hybridization by designing 18mer targets to bind to the 18 bases on 25mer probes closest to the solid support.[14] When, in this manner, the targets were forced to partially penetrate into the DNA layer to initiate hybridization, significantly slower kinetics were observed than when they were designed to bind to the outermost eighteen bases of the probes. Similar slowdown phenomena have been also implicated in other processes involving macromolecules at interfaces. For example, in block copolymer adsorption, the growing layer of adsorbed chains presents an increasingly formidable kinetic barrier to adsorption of later-arriving chains, manifesting in an exponentially decaying rate of approach to equilibrium.[67] If significantly longer time scales can be addressed with our methods[68] it would be interesting to see whether a similar description may apply to kinetics of MO−DNA surface hybridization.

That hybridization to DNA probes was not as susceptible to kinetic limitations is consistent with their different organization. While collapse of MO probes mandates that targets penetrate the duplex layer to reach an available probe partner, DNA probes are expected to distribute their segments more evenly throughout the layer. Therefore, duplex formation can be initiated closer to the boundary with buffer, circumventing the need for targets to diffuse deeply into the probe layer.

The conclusions regarding kinetic limitations for hybridization to MO probes may be also compared to published data on PNA−DNA surface hybridization. Hybridization kinetics for PNA−DNA have been reported to deviate significantly from those predicted by a Langmuir model based on fixed rate constants (e.g., Figure 5 in reference 31; Figure 8 in reference 32), suggesting that the kinetic barrier to hybridization evolves as hybridization proceeds. Moreover, the deviations increase in prominence at salt concentrations below ~0.1 mol L^{-1};[31] therefore, the kinetic limitations appear at ionic strengths comparable to those in our MO−DNA study. As mentioned earlier, PNA probe films are expected to be organized similarly to MO films with unhybridized probes near the solid support and PNA−DNA duplexes segregated to the interface with buffer. We therefore propose that the same mechanism may be responsible for kinetic limitations in the PNA probe system, namely hindered transport of target molecules across the growing layer of PNA−DNA duplexes.

4. Conclusions

Comparison of hybridization between morpholino (MO) and DNA oligomers with that between two DNA strands revealed qualitative differences both for solution and for solid-phase hybridization. In solution, MO−DNA hybridization was independent of buffer molarity C_B in the full range from deionized water to 1 mol L^{-1} pH 7.0 phosphate buffer, in contrast to well-known ionic-strength dependence of DNA−DNA hybridization. The independence on C_B indicates that the net interaction of counterions with the unhybridized strands is comparable to that with the corresponding MO−DNA duplex. In the language of counterion condensation, it implies a negligible change in the number of condensed counterions for the duplex relative to the single-stranded molecules.

Hybridization was also investigated on solid supports, when immobilized MO or DNA probes react with DNA targets from solution. The central differences between surface hybridization to MO or to DNA probes were consistent with the expected molecular organization of these layers as governed by probe solubility. DNA probes are expected to remain well solvated, so that unhybridized probes and DNA−DNA duplexes coexist side by side. On the other hand, uncharged and less soluble MO probes are expected to collapse and aggregate on the solid support; i.e. the probes spatially segregate to the surface while the more soluble MO−DNA duplexes protrude into solution.

Such a segregated structure is argued to have important consequences with regard to dependence of MO−DNA surface

(66) Tinland, B.; Pluen, A.; Sturm, J.; Weill, G. *Macromolecules* **1997**, *30*, 5763.
(67) Motschmann, H.; Stamm, M.; Toprakcioglu, C. *Macromolecules* **1991**, *24*, 3681.
(68) Foremost, we are concerned about stability of the electroactive tags used for readout of probe and target coverages, since ferrocenes are prone to degradation if oxidized. We are evaluating several additional tags and modified experimental protocols to determine whether similar experiments can be performed over durations of a day or longer.

hybridization on probe coverage and buffer molarity. Because contact between duplexes and unhybridized probes is limited, penalties to formation of MO−DNA duplexes due to unfavorable interactions with unhybridized probes are diminished so that hybridization is not strongly affected by probe coverage. At high C_B, 0.33 and 1.0 mol L^{-1}, the dependence on probe coverage is instead consistent with steric limits imposed by duplex−duplex overlap, in agreement with the interpretation that MO−DNA duplexes will mostly interact with other duplexes. In contrast, high probe coverages strongly suppress DNA−DNA hybridization under same conditions of C_B, leading to maximum hybridization at intermediate coverage values. Because increase in buffer molarity does not diminish this suppression, the suppression is attributed to nonelectrostatic penalties from contacts between DNA−DNA duplexes and unhybridized DNA probes.

For C_B of 0.11 mol L^{-1} and below, MO−DNA surface hybridization becomes dependent on buffer molarity, indicating onset of limits imposed by electrostatics rather than by duplex overlap. An initial attempt to attribute these limits to a repulsive surface potential built up from accumulation of DNA targets on the surface was found inconsistent as the surface potential did not correlate well with extent of hybridization. Rather, a simple dimensional analysis indicated that MO−DNA hybridization was limited by kinetic constraints arising from the need for targets to penetrate the layer of previously formed MO−DNA duplexes in order to reach a probe partner. In this mechanism, the dependence on C_B comes from sensitivity of target dimensions to ionic strength—the polyelectrolyte nature of the targets causes them to swell as C_B decreases, hindering their transport across the duplex layer. Comparison with published results on hybridization of peptide nucleic acid (PNA) monolayers to DNA targets indicates that similar effects may arise in PNA−DNA surface hybridization.

Acknowledgment. This project was supported by Award No. R01HG004512 from the National Human Genome Research Institute. We thank Professors James Canary and Nadrian Seeman for insightful discussions regarding MO−DNA melting, and Professor Michael Hagan for clarifications regarding the simulation results of reference 50.

Supporting Information Available: Detailed descriptions of materials, melting curve and cyclic voltammetry data analysis, calculation of surface potentials, and complete ref 25. This material is available free of charge via the Internet at http://pubs.acs.org.

JA100881A